SCIENTIFIC REPORTS

OPEN

SUBJECT AREAS:
QUANTUM OPTICS
APPLIED OPTICS

Received
10 March 2014

Accepted
22 May 2014

Published
18 June 2014

Correspondence and requests for materials should be addressed to S.P.W. (swalborn@if.ufrj.br)

Measuring spatial correlations of photon pairs by automated raster scanning with spatial light modulators

E. C. Paul, M. Hor-Meyll, P. H. Souto Ribeiro & S. P. Walborn

Instituto de Física, Universidade Federal do Rio de Janeiro, Caixa Postal 68528, Rio de Janeiro, RJ 21941-972, Brazil.

We demonstrate the use of a phase-only spatial light modulator for the measurement of transverse spatial distributions of coincidence counts between twin photon beams, in a fully automated fashion. This is accomplished by means of the polarization dependence of the modulator, which allows the conversion of a phase pattern into an amplitude pattern. We also present a correction procedure, that accounts for unwanted coincidence counts due to polarization decoherence effects.

Spatial variables of photon pairs have proven to be a useful tool to investigate quantum entanglement and quantum information[1], particularly due to their high-dimensional nature[2–4], capacity for quantum state engineering[5–7], and application to quantum communication[8,9] and quantum imaging[10–13]. Spatial correlations can be measured by digitizing the detection planes and obtaining a raster graphic of the correlations. This kind of measurement can be accomplished by raster-scanning single-pixel detectors in the transverse plane[14–17], using single-photon sensitive CCD cameras[18–22], with other methods such as compressed sensing[23], or using interferometric techniques[24,25], for instance. These methods involve reconstructing the marginal probability distributions associated to the spatial variables.

The spatial light modulator (SLM) has revolutionized the types of operations that can be implemented on the spatial variables of the field. In general, the SLM applies a user-defined position-dependent phase $S(x, y)$ on the incident wavefront. In this way, it is possible to engineer high-dimensional entangled states[26] and also implement a number of quantum logic gates[27] in the spatial variables. Particular interest has been payed to the orbital angular momentum degrees of freedom, where SLM's have been used to test entanglement[28] and Bell's inequality[29] as well as mutually unbiased bases in six dimensions[30], and to simulate stronger-than-quantum correlations[31]. An interesting aspect of certain types of SLMs is the fact that they can be polarization-dependent, imprinting a phase on the field for–say–horizontal (H) polarization and doing nothing when the polarization is vertical (V). Considering both the polarization and spatial degrees of freedom, the action of the SLM can be described by the operator

$$\mathrm{S} = |V\rangle\langle V| \otimes \mathrm{I} + |H\rangle\langle H| \otimes e^{iS(\mathrm{x},\mathrm{y})}, \tag{1}$$

where I is the identity. Using this coupling, quantum logic gates between polarization and spatial parity qubits have been implemented[32], a qubit coupled to a chaotic quantum harmonic oscillator has been studied[33], a single photon and classical channels have been multiplexed in a few-mode fiber[34], spatial moments have been measured directly[35], and an optical integration algorithm has been performed[36]. In Ref. [37], quantum tomography was performed on the polarization qubit for constant homogeneous phases of the SLM, showing that the SLM implements S with a fidelity of about 92%. The imperfect fidelity is due primarily to a slight decoherence of the polarization induced by the SLM. This decoherence can have a detrimental effect on quantum logic gates, and needs to be corrected in some situations[36].

Here we show that the coupling between the polarization and the spatial degrees of freedom (DOF) can be used to perform spatial raster-scanning of a wavefront with the SLM. In this procedure, a phase slit is scanned across the SLM. This allows one to characterize the spatial profile of the field on the SLM in a fully automated fashion. In our measurements we observe spatially inhomogenous background counts, resulting from imperfections in the SLM. This reduces the visibility or constrast of the reconstructed pattern. We then develop a model for the background counts that originate from the polarization decoherence of the SLM. All

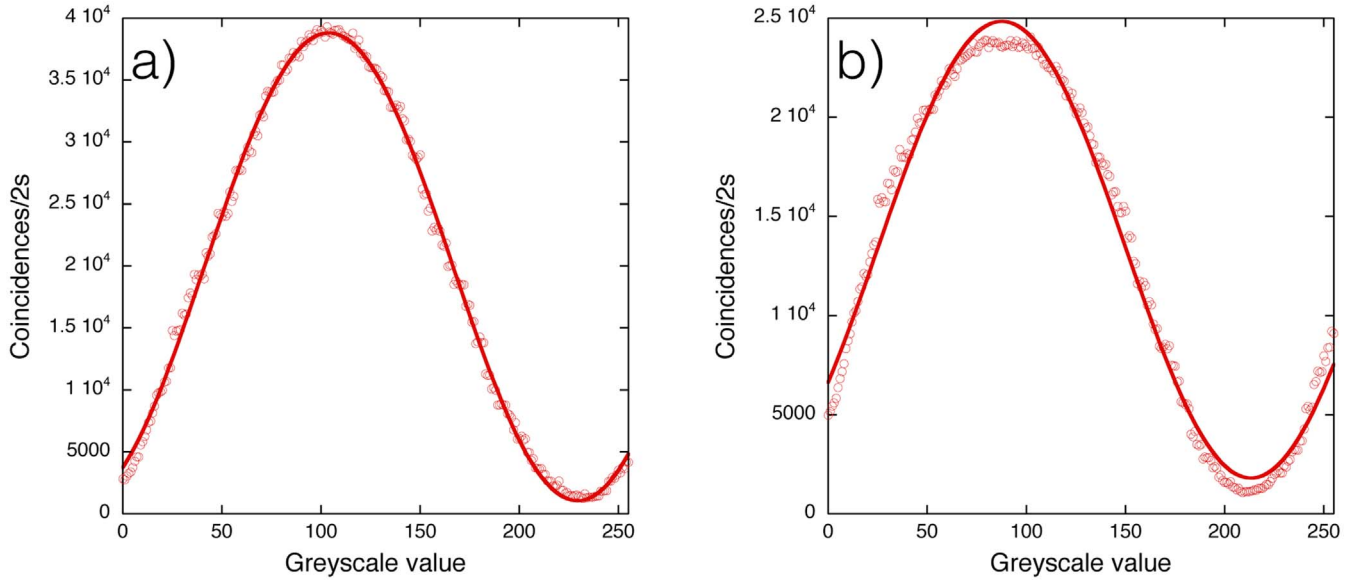

Figure 1 | SLM phase calibration curves. a) Phase calibration curve for photon *s*. b) Phase calibration curve for photon *i*.

parameters from the model can be experimentally determined. Using this model, we can account for the decoherence in such a fashion that the background counts are discarded, thus increasing the contrast of the coincidence distributions.

Raster Scanning with the SLM

Many experiments require the reconstruction of the two-photon coincidence distribution $P(x_s, x_i)$ as a function of the positions x_s and x_i of the signal (s) and idler (i) photons. Traditionally, this has been done by scanning detectors equipped with slit apertures in the transverse plane, using micrometers or stepper motors, as in Refs. [15,17]. More recently, digital micromirrors[4] or single-photon sensitive CCD cameras[18–20] have been used. As an alternative method, we propose to exploit the polarization properties of the SLM. The method consists of producing a series of phase-slit images on the SLM, which are converted into amplitude slits through post-selection of the polarization state of light. This allows for fully automated scanning. To produce a phase pattern with the SLM, an 8 bit (0–255) greyscale image $g(x, y)$ is programmed onto its LCD screen using a computer. An incoming field receives a phase $S(x, y) = 2\pi g(x, y)/256$. To perform a linear scan in the x-axis of the signal beam, we program the SLM with a sequence of N greyscale images I_n composed of phase slits ($n = 0..\ N-1$) of width Δ where the phase pattern is given by

$$a_n(x_s) = \begin{cases} 0 & \text{for } n\Delta \le x_s \le (n+1)\Delta, \\ \pi & \text{elsewhere.} \end{cases} \quad (2)$$

In other words, we program a zero-phase slit of width Δ on the SLM in the region defined above, while all other regions have phase π. A similar phase is applied to the idler beam i, so that we have $b_m(x_i)$, defined in the same way. We consider the two-photon state obtained from spontaneous parametric down-conversion (SPDC) in the paraxial and monochromatic approximations[1]:

$$|\Psi\rangle = \int\int dx_s dx_i \psi(x_s,x_i)|x_s,+\rangle_s|x_i,+\rangle_i, \quad (3)$$

where $|x_j, +\rangle$ refers to a single photon state in the position representation and with the diagonal polarization state: $|+\rangle = \left(1/\sqrt{2}\right)(|H\rangle + |V\rangle)$. Applying the SLM operation S, on both signal and idler beams and projecting onto the $|+\rangle_s|+\rangle_i$ joint polarization state, the coincidence detection probability is

$$P(n,m) = \int_{n\Delta}^{(n+1)\Delta} dx_s \int_{m\Delta}^{(m+1)\Delta} dx_i |\psi(x_s,x_i)|^2. \quad (4)$$

In this way, the entire $N \times N$ two-photon coincidence distribution can be reconstructed. The spatial resolution of this method depends upon the slit width Δ. On the one hand, for large slit width, the reconstructed distribution $P(n, m)$ is strongly discretized, which can cause problems when one wishes to estimate entanglement[38,39]. On the other hand, when the slit width Δ is narrow, unwanted background counts that appear due to imperfections in the operation of the SLM become increasingly more relevant, as we will see explicitly below. In the next section we describe a model for the origin of these background counts and present a post-processing method to reduce them, greatly increasing the fidelity with the true coincidence distribution.

Improved Scanning Method

Programming a constant phase ϕ on the SLM, we can perform a polarization rotation of the form $|+\rangle \rightarrow (|V\rangle + \exp(i\phi)|H\rangle)/\sqrt{2}$, on the incident field. Ideally, a subsequent polarization measurement using a polarizing beam splitter would project this state onto the two orthogonal polarization states $|+\rangle$ and $|-\rangle$ with probabilities $P_+ = \cos^2(\phi/2)$ and $P_- = \sin^2(\phi/2)$. Therefore, measurements of P_+ and P_- give us an interference curve whose phase is defined by the SLM. In Figs. 1a) and b) we show this kind of polarization interference as a function of the uniform greyscale value applied to the SLM. In these measurements, one photon was detected in the $|+\rangle$ polarization state and the other in the $|V\rangle$ polarization state that is unsensitive to the SLM, so as not to interfere with the polarization oscillations of the other photon. In this way, these curves correspond to single-photon interference curves, and provide information about the noise counts that occur due to polarization incoherence.

The visibility is defined as

$$\mathcal{V} = \frac{I_{max} - I_{min}}{I_{max} + I_{min}}, \quad (5)$$

where I is the coincidence count rate. Ideally, $I_{max} = I$, $I_{min} = 0$ and $\mathcal{V} = 1$. However, due to imperfections of the SLM, the visibility is reduced. Fitting the curves with a sinusoidal function, we find $\mathcal{V}_s = 0.947 \pm 0.004$ and $\mathcal{V}_i = 0.87 \pm 0.01$ for the signal and idler

photons, respectively. In principle, the visibilities should be equal. The difference between them is probably due to tiny phase fluctuations in each single pixel[40]. This means that the average noise depends on the effective number of pixels interacting with the beam, and on the transverse field distribution. Therefore, differences in the diameter and intensity distribution of the two beams, may lead to different visibilities.

Let us define p as the probability that the modulation is succesfully applied to a photon field. This means that, at the polarizing beam splitter, the photon is transmitted when the SLM is set to apply a phase zero and reflected when the SLM is set to apply a phase π. Then we have $I_{max} = pI$ and $I_{min} = (1 - p)I$. When $p = 1$, we recover the ideal case. Substituting the expressions for I_{max} and I_{min} into Eq. 5 and rearranging, we find $p = (\mathcal{V}+1)/2$.

Let us see how these interference curves provide information about the scanning measurements. The polarization measurement, together with the ideal phase slit, given by the function $a_n(x_s, y_s)$, defines an aperture described by a rectangle function with transmission 1 in the region $n\Delta \le x \le (n + 1)\Delta$ and 0 otherwise. In practice, due to the less than unity visibility, the effective aperture is a rectangle function with transmission p in the region $n\Delta \le x \le (n + 1)\Delta$ and $(1 - p)$ otherwise. As p can be determined from the visibility $\mathcal{V}$, we can experimentally determine the value of p, and take the decoherence into account.

Let us first describe our model for the simplified case where the SLM surface is divided in 3 slit regions for each light beam, as shown in Fig. 2. We denote C_{ij} as the ideal ($\mathcal{V} = 1$) number of coincidence counts when slit 1 is at position i and slit 2 is at position j. Here 1 and 2 refer to signal and idler, respectively. We define N_{ij} as the measured number of coincidence counts between these two regions. Ideally, for a perfect SLM and perfect polarization optics, we would detect coincidence counts only between photons incident on the phase slits, so that $N_{ij} = C_{ij}$. However, due to the imperfections discussed above, we detect coincidence counts that originate from other regions of the SLM. The probability that a photon is detected when coming from a zero phase region, implementing the equivalent of a slit, is given by the p obtained from the visibility measurements, as explained above. Likewise $(1 - p)$ is the probability that a photon is detected when coming from a region modulated with phase π. Then, we see a decrease in signal, since instead of detecting all ideal counts C_{11} we detect $p_s p_i C_{11} \le C_{11}$ of them. In addition, we detect unwanted counts coming from different combinations of π-phase regions of the SLM. For example, it is possible that photon s reflected from region 1 and photon i from region 2 or 3, contributing to a background term. Then, we expect a contribution from terms C_{12} and C_{13} that is proportional to $p_s(1 - p_i)$. Similarly, terms like C_{22} and C_{23} appear with a proportionality constant $(1 - p_s)(1 - p_i)$. Summing up all these events, we can relate the measured count rate N_{11} to the ideal count rates as

$$N_{11} = p_s p_i C_{11} + p_s(1-p_i)(C_{12}+C_{13}) + (1-p_s)p_i(C_{21}+C_{31}) + (1-p_s)(1-p_i)(C_{22}+C_{23}+C_{32}+C_{33}). \quad (6)$$

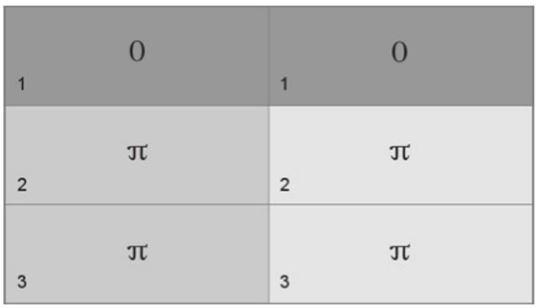

Figure 2 | Phase slits on the SLM for measurement of coincidences N_{11}.

Let us arrange the measured and ideal coincidence counts as column vectors:

$$\mathbf{N} = \begin{pmatrix} N_{11} \\ N_{12} \\ N_{13} \\ N_{21} \\ N_{22} \\ N_{23} \\ N_{31} \\ N_{32} \\ N_{33} \end{pmatrix} \quad \text{and} \quad \mathbf{C} = \begin{pmatrix} C_{11} \\ C_{12} \\ C_{13} \\ C_{21} \\ C_{22} \\ C_{23} \\ C_{31} \\ C_{32} \\ C_{33} \end{pmatrix}. \quad (7)$$

We can write the measured coincidence counts $\mathbf{N}$ as a function of the ideal coincidence counts $\mathbf{C}$ as

$$\mathbf{N} = \mathbf{E}\mathbf{C}, \quad (8)$$

where the symmetric matrix

$$\mathbf{E} = \begin{pmatrix} \alpha & \gamma & \gamma & \delta & \beta & \beta & \delta & \beta & \beta \\ \gamma & \alpha & \gamma & \beta & \delta & \beta & \beta & \delta & \beta \\ \gamma & \gamma & \alpha & \beta & \beta & \delta & \beta & \beta & \delta \\ \delta & \beta & \beta & \alpha & \gamma & \gamma & \delta & \beta & \beta \\ \beta & \delta & \beta & \gamma & \alpha & \gamma & \beta & \delta & \beta \\ \beta & \beta & \delta & \gamma & \gamma & \alpha & \beta & \beta & \delta \\ \delta & \beta & \beta & \delta & \beta & \beta & \alpha & \gamma & \gamma \\ \beta & \delta & \beta & \beta & \delta & \beta & \gamma & \alpha & \gamma \\ \beta & \beta & \delta & \beta & \beta & \delta & \gamma & \gamma & \alpha \end{pmatrix},$$

and $\alpha = p_s p_i$, $\beta = (1 - p_s)(1 - p_i)$, $\gamma = p_s(1 - p_i)$, $\delta = (1 - p_s)p_i$. Finding the inverse of this matrix $\mathbf{E}^{-1}$, we can find the ideal coincidence counts as a function of the measured counts

$$\mathbf{C} = \mathbf{E}^{-1}\mathbf{N}. \quad (9)$$

In the more general case of d slit positions, we follow the same procedure as outlined above, to obtain

$$N_{ij} = \alpha C_{ij} + \beta \sum_{\substack{m \neq i \\ n \neq j}} C_{mn} + \gamma \sum_{n \neq j} C_{in} + \delta \sum_{m \neq i} C_{mj}, \quad (10)$$

and the matrices $\mathbf{E}$ and $\mathbf{E}^{-1}$ are described accordingly.

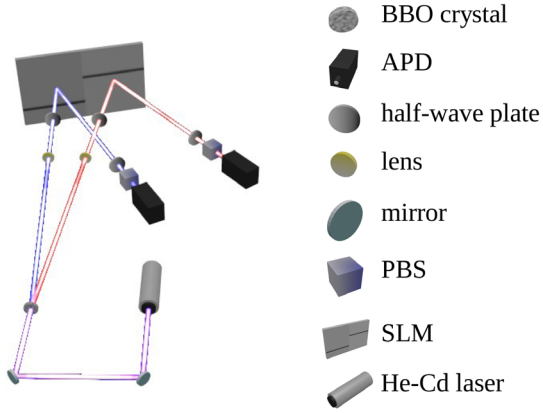

Figure 3 | Experimental setup. Signal (blue) and idler (red) beams are directed onto the SLM. As can be seen in the image, each of the twin photons is incident on one side of the SLM. Acronyms are defined in the text.

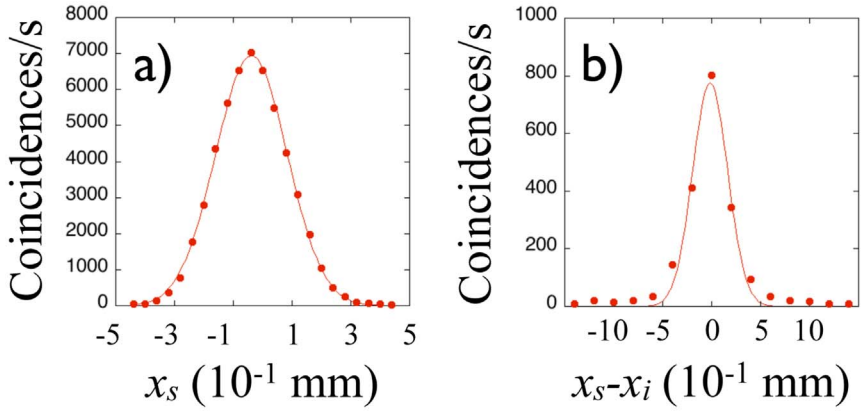

Figure 4 | Experimental results when the detectors are scanned in the transverse plane. a) The marginal coincidence distribution $C_s(x_s)$. b) The marginal coincidence distribution $C_-(x_s - x_i)$.

Experiment

Figure 3 shows a sketch of the experimental setup. Horizontally polarized frequency-degenerate twin photons at 650 nm are generated by pumping a non-linear BBO (β-Barium Borate) crystal with a He-Cd laser operating at $\lambda = 325$ nm. The photons are directed onto a single SLM using mirrors and lenses. The SLM is the Pluto reflective phase-modulation-only model fabricated by Holoeye, with resolution 1920 × 1080 pixels and 8.0-μm pixel pitch. A half-wave plate is used right before the SLM to prepare the polarization state of the photons to $|+\rangle$. At the detection stage, each beam goes through another wave plate and a polarizing beam splitter to select the photons that reflected off of the intended region of the SLM. The detectors are single-photon avalanche photodiodes (APD) with large detection aperture. Lenses (focal lengths 70 cm and 15 cm) are used to map the tranverse position of the down-converted beams onto the SLM. For the measurements, horizontal phase slits are scanned vertically on each half of the SLM, corresponding to each beam. The total scan region for each photon is thus 1080 pixels.

Results

In order to characterize the spatial distribution of the coincidence counts in the absence of the SLM, we first performed the traditional procedure of scanning the detectors in the transverse plane and registering coincidence counts as a function of the detector position x. In these measurements the scanning detectors were equipped with a 20-μm slit aperture and scanned in the vertical direction. The polarization of the photons was set to the vertical direction, so that the SLM had no effect on the spatial distribution. Figure 4a) shows results when detector D_s is scanned and detector D_i is completely open (area-integrating). Fig. 4b) shows results when the detectors are scanned in opposite directions, giving the coincidence distribution as a function of $x_s - x_i$. The data of both figures fit well to gaussian functions. We also see that the tails of the gaussians go to zero, indicating low background counts outside the coincidence region.

Next we performed scanning measurements, this time using the SLM as described in the previous section. Figure 5 shows several two-dimensional scans, obtained by scanning in the vertical direction of the signal and idler photons. The scans were performed using phase

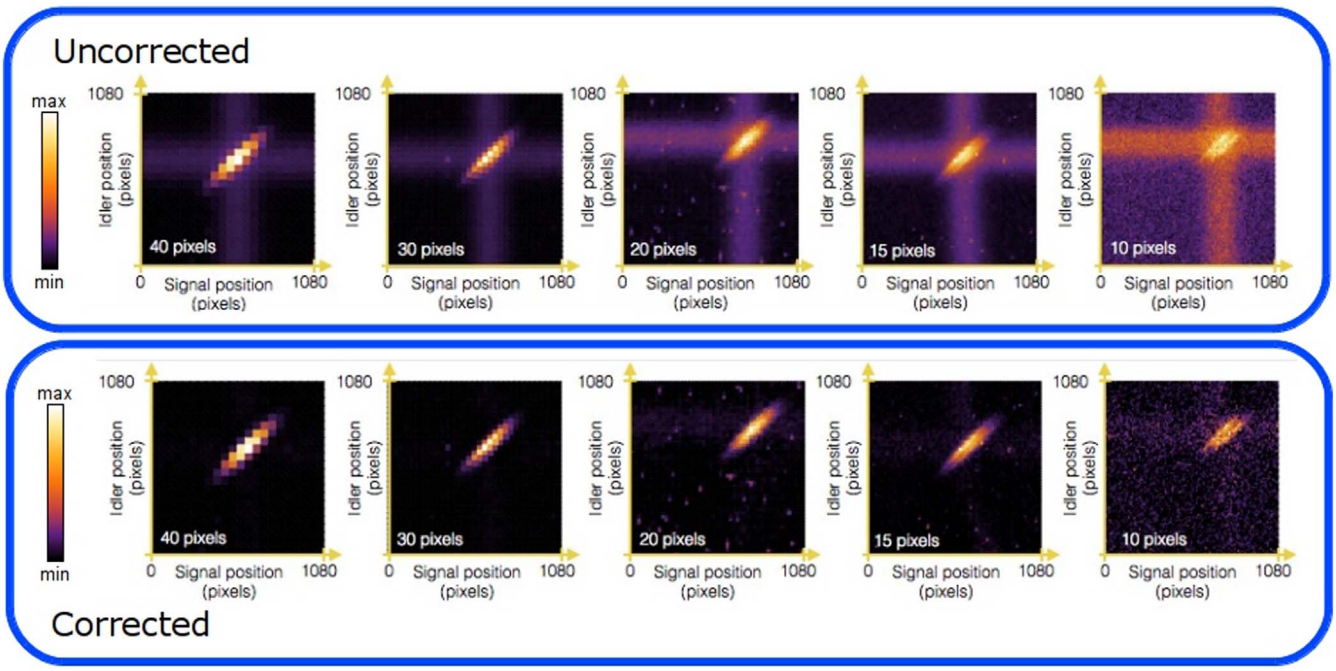

Figure 5 | Experimental results for 2D scans. The top row corresponds to raw data, giving distributions **N**. The bottom row corresponds to corrected data **C**. The splitting of the elliptical shapes seen in the smaller slit widths is probably due to the mapping of the intensity distribution of the pump-laser beam, which happens when the coincidences are measured in the near field.

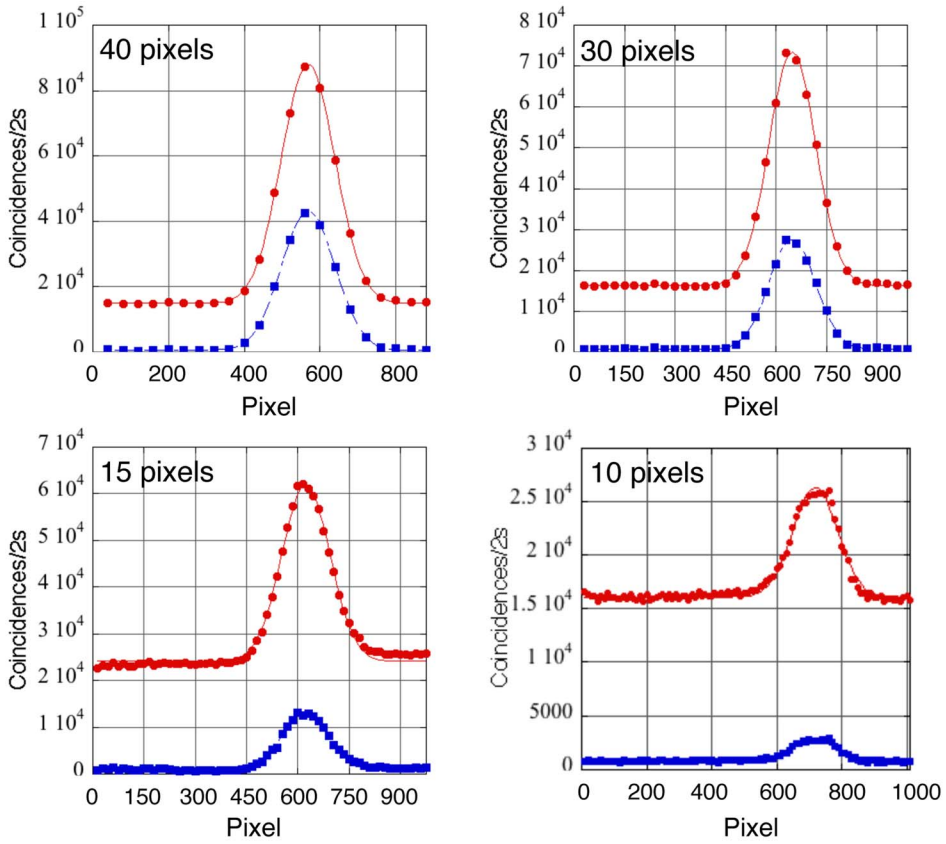

Figure 6 | Experimental results for the marginal distributions of the signal photon. Red circles correspond to raw data $\mathbf{N_s}$, and blue circles to data processed according to the procedure described in the paper, giving $\mathbf{C_s}$.

slits of widths: 40, 36 (not shown), 30, 20, 15 and 10 pixels, as depicted in the different graphs. In all measurements (with SLM and with scanning detectors) accidental-coincidence count rates, defined as $C_{acc} = c_s c_i \Delta t$, were subtracted. In this formula, c_s and c_i are the detector single-photon count rates and Δt is the temporal coincidence window. The upper row shows the raw uncorrected data, giving the raw distributions **N**. The usual elliptical pattern showing spatial correlations can be seen. As the slit width decreases in size, an increasingly prominent background contribution can be observed, which appears as the cross-shaped pattern covering the entire scanning region. It can be seen that the contrast decreases as the slit size decreases. The lower row of Figure 5 shows the data when the correction procedure described above has been applied, giving the corrected distributions **C**. We can observe that the background counts are greatly reduced. The correction procedure is less effective for smaller slit sizes, where the signal-to-noise ratio is smaller. As the phase noise in the SLM is time dependent[40] within the millisecond range, this noise is more effective when the photon flux is small.

To better observe the reduction in background counts, in Figure 6 we show one-dimensional marginal distributions for only the signal photon as a function of the slit position. Red circles correspond to uncorrected data $\mathbf{N}_s$ and blue squares to corrected data $\mathbf{C}_s$. Gaussian curve fits serve as a guide to the eye. We observe that the inhomogenous background contribution, represented by the flat tails of the gaussian distributions, is nearly eliminated in the corrected measurements. These plots can be compared to Fig. 4a), which was obtained by scanning the detector D_1 directly. Using the distribution shown in Fig. 4a), we calculate the variance of the distributions $C_s(x_s)$ on the SLM, giving $\langle \Delta x_s^2 \rangle = (5274 \pm 170)$ pixels^2. Converting the width of the mechanical slit in terms of the dimensions of the SLM pixels, and taking into account the magnification of the optical system, the result obtained is nearly 13 pixels. Therefore, we compare it to the variance of the corrected distribution obtained with a 15 pixel width phase slit, obtaining (5771 ± 380) pixels^2, showing compatibility to within experimental error. Calculating the variance directly from the uncorrected data gives a value that is incorrect by several orders of magnitude.

To quantify the improvement in background counts, we define the contrast $\mathcal{C} = c_{max}/c_{tail}$, where c_{max} is the count rate at the maximum of the gaussian, and c_{tail} is the nearly constant count rate at the flat tail

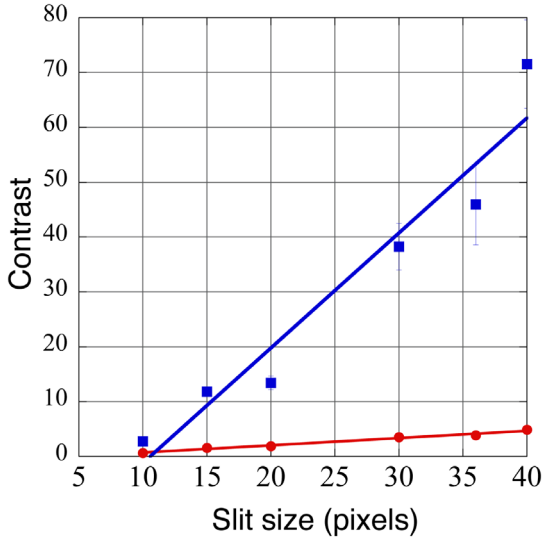

Figure 7 | Contrast as a function of the width of the phase slit, for uncorrected measurements $\mathbf{N_s}$ (red circles) and corrected measurements $\mathbf{C_s}$ (blue squares).

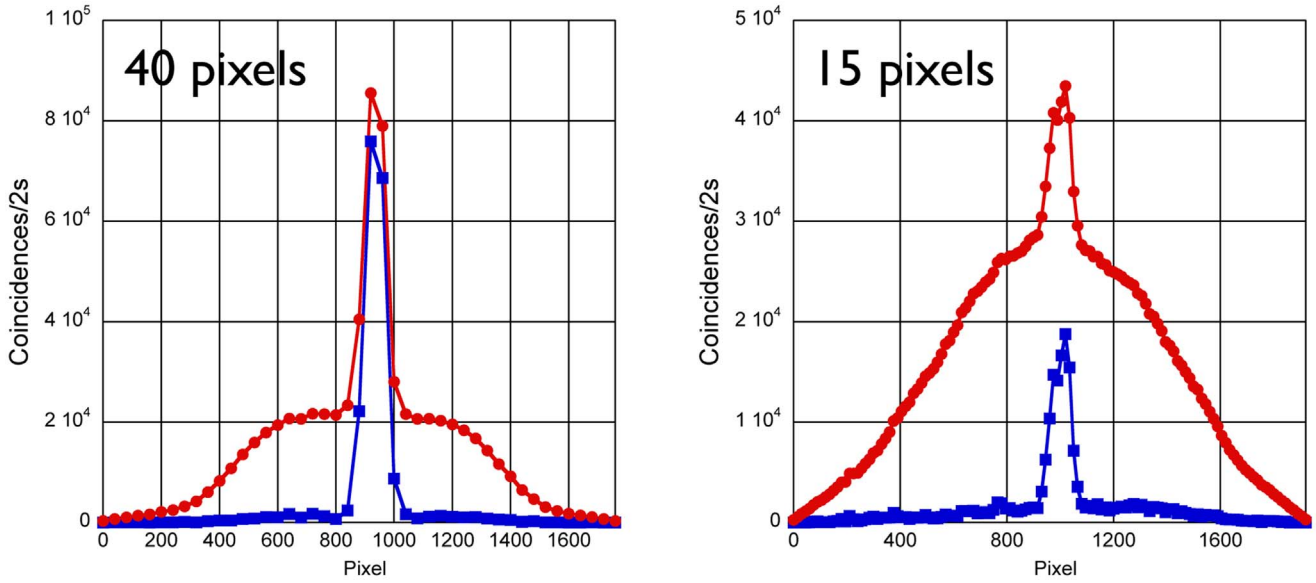

Figure 8 | Marginal distributions for the anti-diagonal coordinate $x_s - x_i$. Red circles correspond to raw data, giving distribution $\mathbf{N}_-$, and blue squares correspond to corrected data, giving distribution $\mathbf{C}_-$.

of the gaussian distribution. In Figure 7 we plot the contrast for both uncorrected and corrected measurements as a function of the slit size, and do a linear fit to the data. The ratio of the slopes of the lines is about 15.75, showing that we obtained an improvement in the contrast of more than an order of magnitude for the corrected data.

By summing the coincidence distributions ($\mathbf{N}$ or $\mathbf{C}$) over the diagonal variable $x_s + x_i$, we have the marginal coincidence distributions $\mathbf{N}_-$ and $\mathbf{C}_-$ for the anti-diagonal variable $x_s - x_i$, as shown in Fig. 8. Red circles correspond to raw data $\mathbf{N}_-$ and blue squares to corrected data $\mathbf{C}_-$. We can see that the corrected data more closely approximates the distribution $C(x_s - x_i)$ shown in Fig. 4b).

Our method is the simplest correction, in the sense that we assume that the value of p_s (p_i) is the same for all pixels of the signal (idler) photon. We believe that more sophisticated methods are also viable, if one takes into account more technical details about the SLM.

Conclusion

In conclusion, we have presented a method for performing scanning measurements of spatial correlations of photons using an imperfect phase-only SLM. Exploiting the polarization dependence of the device, we use polarization interference measurements to turn a phase mask into an amplitude mask. We present a model that takes into account inhomogenous background counts introduced by the SLM and other imperfections in the system. We observe a considerable increase in contrast. We show that our method is useful for characterizing and studying spatial correlations of photon pairs.

1. Walborn, S. P., Monken, C. H., Pádua, S. & Souto Ribeiro, P. H. Spatial correlations in parametric down-conversion. *Phys. Rep.* **495**, 87–139 (2010).
2. Law, C. K. & Eberly, J. H. Analysis and interpretation of high transverse entanglement in optical parametric down conversion. *Phys. Rev. Lett.* **92**, 127903 (2004).
3. Straupe, S. S., Ivanov, D. P., Kalinkin, A. A., Bobrov, I. B. & Kulik, S. P. Angular Schmidt modes in spontaneous parametric down-conversion. *Phys. Rev. A* **83**, 060302 (2011).
4. Dixon, P. B., Howland, G. A., Schneeloch, J. & Howell, J. C. Quantum mutual information capacity for high-dimensional entangled states. *Phys. Rev. Lett.* **108**, 143603 (2012).
5. Nogueira, W. A. T., Walborn, S. P., Pádua, S. & Monken, C. H. Generation of a two-photon singlet beam. *Phys. Rev. Lett.* **92**, 043602 (2004).
6. Neves, L. *et al.* Generation of entangled states of qudits using twin photons. *Phys. Rev. Lett.* **94**, 100501 (2005).
7. Yarnall, T., Abouraddy, A. F., Saleh, B. E. A. & Teich, M. C. Experimental violation of Bell's inequality in spatial-parity space. *Phys. Rev. Lett.* **99**, 170408 (2007).
8. Zhang, L., Silberhorn, C. & Walmsley, I. A. Secure quantum key distribution using continuous variables of single photons. *Phys. Rev. Lett.* **100**, 110504 (2008).
9. Pereira, M. V. C., Filpi, L. A. P. & Monken, C. H. Cancellation of atmospheric turbulence effects in entangled two-photon beams. *Phys. Rev. A* **88**, 053836 (2013).
10. Fonseca, E. J. S., Monken, C. H. & Pádua, S. Measurement of the de Broglie wavelength of a multiphoton wave packet. *Phys. Rev. Lett.* **82**, 2868 (1999).
11. Abouraddy, A. F., Saleh, B. E. A., Sergienko, A. V. & Teich, M. C. Role of entanglement in two-photon imaging. *Phys. Rev. Lett.* **87**, 123602 (2001).
12. Bennink, R. S., Bentley, S. J., Boyd, R. W. & Howell, J. C. Quantum and classical coincidence imaging. *Phys. Rev. Lett.* **92**, 033601 (2004).
13. Abouraddy, A. F., Stone, P. R., Sergienko, A. V., Saleh, B. E. A. & Teich, M. C. Entangled-photon imaging of a pure phase object. *Phys. Rev. Lett.* **93**, 213903 (2004).
14. D'Angelo, M., Kim, Y.-H., Kulik, S. P. & Shih, Y. Identifying entanglement using quantum ghost interference and imaging. *Phys. Rev. Lett.* **92**, 233601 (2004).
15. Howell, J. C., Bennink, R. S., Bentley, S. J. & Boyd, R. W. Realization of the Einstein-Podolsky-Rosen paradox using momentum- and position-entangled photons from spontaneous parametric down conversion. *Phys. Rev. Lett.* **92**, 210403 (2004).
16. Tasca, D. S., Walborn, S. P., Souto Ribeiro, P. H. & Toscano, F. Detection of transverse entanglement in phase space. *Phys. Rev. A* **78**, 010304 (2008).
17. Tasca, D. S., Walborn, S. P., Souto Ribeiro, P. H., Toscano, F. & Pellat-Finet, P. Propagation of transverse intensity correlations of a two-photon state. *Phys. Rev. A* **79**, 033801 (2009).
18. Abouraddy, A. F., Nasr, M. B., Saleh, B. E. A., Sergienko, A. V. & Teich, M. C. Demonstration of the complementarity of one- and two-photon interference. *Phys. Rev. A.* **63**, 063803 (2001).
19. Edgar, M. P. *et al.* Imaging high-dimensional spatial entanglement with a camera. *Nat. Commun.* **3**, 984 (2012).
20. Aspden, R. S., Tasca, D. S., Boyd, R. W. & Padgett, M. J. EPR-based ghost imaging using a single-photon-sensitive camera. *New J. Phys.* **15**, 073032 (2013).
21. Tasca, D. S., Edgar, M. P., Izdebski, F., Buller, G. S. & Padgett, M. J. Optimizing the use of detector arrays for measuring intensity correlations of photon pairs. *Phys. Rev. A* **88**, 013816 (2013).
22. Fickler, R., Krenn, M., Lapkiewicz, R., Ramelow, S. & Zeilinger, A. Real-time imaging of quantum entanglement. *Sci. Rep.* **3**, 1914 (2013).
23. Howland, G. A. & Howell, J. C. Efficient high-dimensional entanglement imaging with a compressive-sensing double-pixel camera. *Phys. Rev. X* **3**, 011013 (2013).
24. Chan, K. W., Torres, J. P. & Eberly, J. H. Transverse entanglement migration in Hilbert space. *Phys. Rev. A* **75**, 050101 (2007).
25. Just, F., Cavanna, A., Chekhova, M. V. & Leuchs, G. Transverse entanglement of biphotons. *New J. Phys.* **15**, 083015 (2013).
26. Lima, G., Vargas, A., Neves, L., Guzmán, R. & Saavedra, C. Manipulating spatial qudit states with programmable optical devices. *Opt. Express* **17**, 10688–10696 (2009).
27. Tasca, D. S., Gomes, R. M., Toscano, F., Souto Ribeiro, P. H. & Walborn, S. P. Continuous-variable quantum computation with spatial degrees of freedom of photons. *Phys. Rev. A* **83**, 052325 (2011).
28. Leach, J. *et al.* Quantum correlations in optical angleorbital angular momentum variables. *Science* **329**, 662 (2010).

29. Dada, A. C., Leach, J., Buller, G. S., Padgett, M. J. & Andersson, E. Experimental high-dimensional two-photon entanglement and violations of generalized Bell inequalities. *Nat. Phys.* **7**, 677–680 (2011).
30. D'Ambrosio, V. *et al*. Test of mutually unbiased bases for six-dimensional photonic quantum systems. *Sci. Rep.* **3**, 2726 (2013).
31. Romero, J., Giovannini, D., Tasca, D. S., Barnett, S. & Padgett, M. J. Tailored two-photon correlation and fair-sampling: a cautionary tale. *New J. Phys.* **15**, 083047 (2014).
32. Abouraddy, A. F., Di Giuseppe, G., Yarnall, T. M., Teich, M. C. & Saleh, B. E. A. Implementing one-photon three-qubit quantum gates using spatial light modulators. *Phys. Rev. A* **86**, 050303 (2012).
33. Lemos, G. B., Gomes, R. M., Walborn, S. P., Souto Ribeiro, P. H. & Toscano, F. Experimental observation of quantum chaos in a beam of light. *Nat. Commun.* **3**, 1211 (2012).
34. Carpenter, J. *et al*. Mode multiplexed single-photon and classical channels in a few-mode fiber. *Opt. Express* **21**, 28794 (2013).
35. Hor-Meyll, M., Almeida, J. O., Lemos, G. B., Souto Ribeiro, P. H. & Walborn, S. P. Ancilla-assisted measurement of photonic spatial correlations and entanglement. *Phys. Rev. Lett.* **112**, 053602 (2014).
36. Lemos, G. B., Souto Ribeiro, P. H. & Walborn, S. P. Optical integration of a real-valued function by measurement of a Stokes parameter. *J. Opt. Soc. Am. A* **31**, 704–707 (2014).
37. Lemos, G. B., Almeida, J. O., Walborn, S. P., Souto Ribeiro, P. H. & Hor-Meyll, M. Characterization of a spatial light modulator as a polarization quantum channel. *Phys. Rev. A* **89**, 042119 (2014).
38. Schneeloch, J., Dixon, P. B., Howland, G. A., Broadbent, C. J. & Howell, J. C. Violation of continuous-variable Einstein-Podolsky-Rosen steering with discrete measurements. *Phys. Rev. Lett.* **110**, 130407 (2013).
39. Tasca, D. S., Rudnicki, L., Gomes, R. M., Toscano, F. & Walborn, S. P. Reliable entanglement detection under coarse-grained measurements. *Phys. Rev. Lett.* **110**, 210502 (2013).
40. Lizana, A. *et al*. Time fluctuations of the phase modulation in a liquid crystal on silicon display: characterization and effects in diffractive optics. *Opt. Express* **16**, 16711–16722 (2008).

Acknowledgments

We acknowledge financial support from the Brazilian agencies CNPq, FAPERJ, CAPES and the INCT-Informação Quântica.

Author contributions

E.C.P., M.H.-M., P.S.R. and S.P.W. conceived the main idea and wrote the manuscript, E.C.P. performed the experiment, E.C.P. and S.P.W. analyzed the data and prepared the figures.

Additional information

Competing financial interests: The authors declare no competing financial interests.

How to cite this article: Paul, E.C., Hor-Meyll, M., Souto Ribeiro, P.H. & Walborn, S.P. Measuring spatial correlations of photon pairs by automated raster scanning with spatial light modulators. *Sci. Rep.* **4**, 5337; DOI:10.1038/srep05337 (2014).